Journal of Non-Crystalline Solids 385 (2014) 111–116

Contents lists available at ScienceDirect

Journal of Non-Crystalline Solids

journal homepage: www.elsevier.com/ locate/ jnoncrysol

Crystallization kinetics and thermal stability of mechanically alloyed $Al_{76}Ni_8Ti_8Zr_4Y_4$ glassy powder

Xinfu Wang, Dan Wang, Bo Zhu, Yunjie Li, Fusheng Han *

Key Laboratory of Materials Physics, Institute of Solid State Physics, Chinese Academy of Sciences, Hefei, Anhui 230031, China

ARTICLE INFO

Article history:
Received 14 September 2013
Received in revised form 3 November 2013
Available online 28 November 2013

Keywords:
Mechanical alloying;
Glassy powder;
Crystallization;
Thermal stability

ABSTRACT

$Al_{76}Ni_8Ti_8Zr_4Y_4$ glassy powder was produced by mechanical alloying process. The phase structure and the crystallization kinetics as well as the thermal stability were investigated using X-ray diffraction (XRD), transmission electron microscopy (TEM) and differential scanning calorimeter (DSC) in non-isothermal mode. The glassy alloy powder shows a distinct one-stage crystallization process with a wide supercooled liquid region. Crystallization occurs by the precipitation and growth of FCC-Al, with intermetallic compound AlTi, $AlTi_3$, Al_2Y and Al_3Zr. The non-isothermal crystallization kinetics is analyzed by the modified Johnson–Mehl–Avrami (JMA) equation. The values of the Avrami exponent imply that the dominating crystallization mechanism of the present glassy powder is two- or three-dimensional nucleation and growth controlled by diffusion of atoms. The present glass powder has a large supercooled liquid region (SLR) ΔT_x value (86 K) and the apparent activation energy for crystallization is as high as 316 kJ/mol. The thermal stability was also evaluated by continuous transformation diagram (CHT) obtained by the extended Kissinger equation. To convince the thermal stability for a very long period of time, a quick annealing of the glassy powder at 700 K for 24 h was conducted and the related result was discussed.

1. Introduction

Al-based metallic glasses (MGs) have attracted continuing attentions for decades, owing to their outstanding properties, such as low density, high strength, high elastic strain limit and good corrosion resistance [1–6], which make them suitable for structural applications in the transportation and aviation industry. However, their low glass forming ability has hindered the fabrication of Al-based bulk metallic glasses (BMGs) by conventional casting processes [3,4]. So far, Al-based metallic glasses are still obtained mostly in thin ribbons [5,6], and the maximum thickness of the Al-based bulk metallic glass material fabricated by rapid cooling method available is about 1 mm [7], which means that the application of Al-based metallic glasses as a structural material has been restricted.

As is known, mechanical alloying (MA) is a very convenient solid-state synthesis alternative to rapid quenching, melt spinning, and gas atomization techniques for synthesizing a wide range of novel materials including amorphous or nanocrystalline products [3–5,8,9]. Based on the glassy powders produced by MA, the bulk glasses can be produced via powder metallurgy route such as the spark plasma sintering (SPS) process and equal channel angular extrusion in the SLR [10–14], which makes it possible to produce bulk metallic glasses in more extensive ranges of size and shape [15]. However, the most significant problem of consolidation of glassy powders arises from the risk of possible crystallization during high temperature exposure. Therefore, to take advantage of the PM approach for the fabrication of Al-based BMGs, it is necessary to clearly understand the thermal stability and the crystallization kinetics of the glassy powders. The higher thermal stability of the glassy powders, the better for fabrication of BMGs. Efforts have been made to improve the thermal stability of amorphous alloys [16–18]. Generally, the thermal stability of glassy alloys can be improved by inhibiting the nucleation for the primary phase, and the addition of rare earth element and high melting points early transition metals are suggested to be an effective way to impose the resistance of the atom diffusion. In particular, addition of large atoms, such as Y, is very helpful in terms of thermal stability [18]. Meanwhile, Y was useful for the passivation of oxygen in chemistry and restrained the negative effect of oxygen.

In this contribution, the present work demonstrates the synthesis of $Al_{76}Ni_8Ti_8Zr_4Y_4$ amorphous powder by MA of elemental powder mixtures. The composition of $Al_{76}Ni_8Ti_8Zr_4Y_4$ was obtained by slightly increasing the Al content of the glass-forming $Al_{75}Ni_{10}Ti_{10}Zr_5$ alloy [19], while keeping the ratios between the remaining elements constant, namely, the Al content was increased to 76 at.%, Ni, Ti, and Zr contents were reduced to 8 at.%, 8 at.%, 4 at.%, respectively, and the Y content was correspondingly increased to 4 at.%. The structural evolution and the effect of Y addition on the thermal stability as well as crystallization kinetics of Al–Ni–Ti–Zr–Y alloys are examined, aiming at clarifying the amorphization process of the $Al_{76}Ni_8Ti_8Zr_4Y_4$ glassy powder and giving fundamentals for the proceeded consolidation and crystallization processes.

* Corresponding author. Tel.: +86 551 65591435; fax: +86 551 65591434.
E-mail address: fshan@issp.ac.cn (F. Han).

0022-3093/$ – see front matter © 2013 Elsevier B.V. All rights reserved.
http://dx.doi.org/10.1016/j.jnoncrysol.2013.11.015

2. Experimental

Elemental pure metal powders (99.9% purity) of Al, Ni, Ti, Zr and Y were mixed in the desired nominal composition (at.%) of $Al_{76}Ni_8Ti_8Zr_4Y_4$. The MA process was conducted in a planetary ball mill (QM-3SP4J) operated at 400 rpm using stainless steel vial and bearing balls with a ball to powder weight ratio of 20:1 in an argon atmosphere. 2 wt.% stearic acid was used as a process control agent (PCA) to prevent strong agglomeration of powder particles and sticking to the milling tools. To avoid oxidation, all the powders were handled in a glove box under argon atmosphere. When the pot rotated, cold air was blown over it to avoid elevated temperatures. The MA process was interrupted at giving times to remove the powders cold-welded on the vial wall and to break the agglomerated powders. A small amount of powders was taken out at the predetermined time intervals for structure analysis by means of XRD using Cu Kα radiation (X' Pert Pro MPD). The operation of the powders was also performed in a glove box with a high purity argon gas environment to minimize contamination. The authenticity of XRD analysis concerning the amorphous phase was verified by TEM using a JEOL 2010 with an accelerating voltage of 200 kV. The samples for TEM observation were dispersed into pure ethanol solution first, and then oscillated by supersonic apparatus for 10 min before dropping onto a copper mesh coated with a carbon film. The crystallization kinetic and thermal stability of the powders were evaluated by differential scanning calorimetry (DSC, Pyris Diamond) under non-isothermal conditions in a nitrogen atmosphere at different heating rates, where alumina cups were used as containers. So as to investigate the crystallization behavior and the thermal stability for a very long period of time, the sample was annealed in a tube resistance electric furnace filled with flowing high purity argon at 796 K for 2 h and 700 K for 24 h, respectively. The structure of the annealed sample was determined by X-ray diffraction.

3. Results and discussion

Fig. 1 shows the XRD patterns of $Al_{76}Ni_8Ti_8Zr_4Y_4$ powders after different milling times. It indicates that the characteristic peaks of aluminum, nickel, titanium zirconium, and yttrium elements gradually decreased in intensity and broadened with milling time. The diffuse hump peak can be observed in the 2θ range from 35 to 45° on the XRD patterns after milling for 80 h, suggesting the formation of a kind of nearly full amorphous structure in the alloy. There isn't any crystalline peak being detected within the resolution limit of the XRD as the milling time prolonged to 120 h. The evolution process of the amorphous is as follows: Firstly, Ni dissolves in Al to form Al–Ni solid solution and intermetallic compounds. Secondly, Ti and Y dissolve in Al–Ni solid solution. Finally, Zr dissolves in Al–Ni–Ti–Y solid solution. Such dissolution essentially leads to gradual amorphization of the solid solution. The inset in Fig. 1 illustrates the TEM image of the mechanically alloyed $Al_{76}Ni_8Ti_8Zr_4Y_4$ glassy powder milled for 120 h. The featureless high magnification image and the halo ring with absence of rings in the corresponding SAED pattern are typical for amorphous structure, being in good agreement with the XRD pattern shown in Fig. 1.

Fig. 2 shows the XRD patterns of product phases of the sample annealed at 796 K for 2 h. The crystallization products are FCC Al, AlTi, $AlTi_3$, Al_2Y and Al_3Zr. The formation of several phases having different compositions compared to the glassy phase during devitrification indicates that diffusion of atoms takes place in the crystallization process. Such crystallization of amorphous phases of the alloy into FCC Al and a number of intermetallic compounds is in good agreement with the earlier investigations [20].

The DSC curves of amorphous $Al_{76}Ni_8Ti_8Zr_4Y_4$ powders milled for 120 h at a heating rate of 30 K/min are given in Fig. 3. As is seen, the curves exhibit clear endothermic event, characteristic of a glass transition, followed a wide supercooled liquid region, as well as one pronounced exothermic peak, corresponding to one-step crystallization of the amorphous structure. The crystallization temperature range is 800–840 K with a peak crystallization temperature (T_x^{peak}) of 817 K (heating rate 30 K/min). The specific parameters of the glass transition temperature (T_g), onset crystallization temperatures (T_x^{onset}) and T_x^{peak} are listed in Table 1. It also shows that the glass transition temperature, onset crystallization temperature and peak crystallization temperature shifted to high temperature while the SLR $\Delta T_x = T_x^{onset} - T_g$ decreased from 86 K to 58 K as the heating rate increased, suggesting that the glass transition was delayed to higher temperature. The heating rate dependence of crystallization is caused by the fact that nucleation is a thermally activated process, whereas the kinetics behavior of glass transition is due to the relaxation processes in the glass transition region.

Compared with the non-Y $Al_{75}Ni_{10}Ti_{10}Zr_5$ alloy [19] and the other Al-based amorphous alloys [21,22], the crystallization temperature of the present alloy is higher, which indicates the higher thermal stability of the present amorphous alloy to some extent. It could be explained by appropriate atomic-size mismatch and large negative heat of mixing among constituent elements. Table 2 shows the atomic radii (nm) of the various elements involved in the current study and also the heat of mixing (ΔHm) for the pairs of atomic species. It can be seen that the values of the atomic radius difference (ΔR/R) between Al and Ti

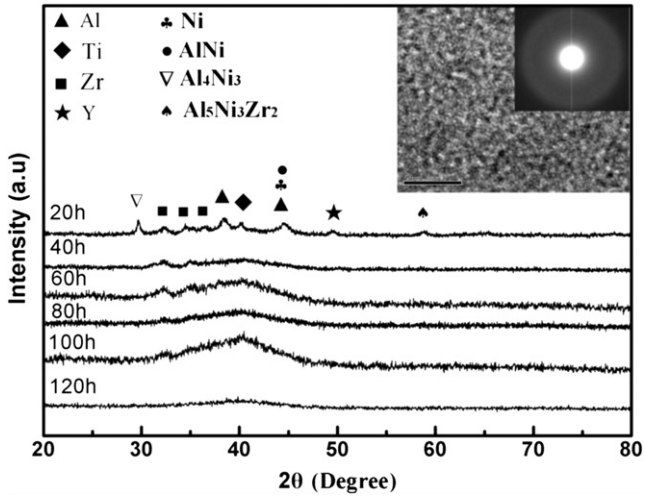

Fig. 1. XRD patterns of the $Al_{76}Ni_8Ti_8Zr_4Y_4$ glassy powder milled for varied times, with TEM images in the inset.

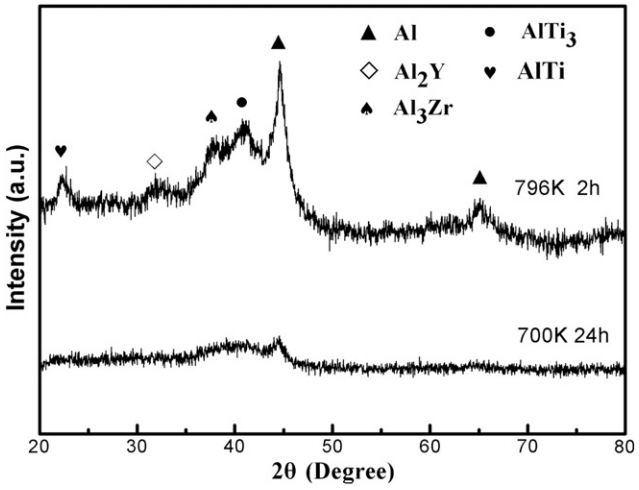

Fig. 2. XRD pattern of $Al_{76}Ni_8Ti_8Zr_4Y_4$ glassy powder milled for 120 h and then annealed at 796 K for 2 h and 700 K for 24 h, respectively.

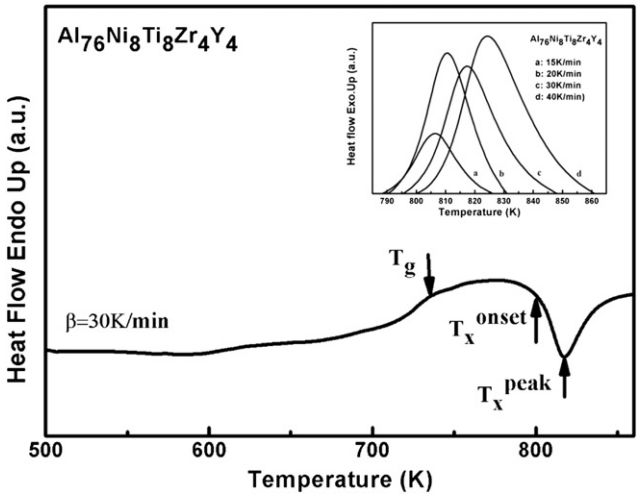

Fig. 3. DSC curves of $Al_{76}Ni_8Ti_8Zr_4Y_4$ glassy powder milled for 120 h at a heating rate of 30 K/min. The inset is the shift of peak crystallization temperature at different heating rates of 15, 20, 30, and 40 K/min.

and Zr is less than 12%, yet the ΔR/R between Y and Al, Ni, and Ti is all greater than 12%. The larger ΔR/R caused by large-size Y addition increases the atomic-size mismatch and give rise to higher packing density, therefore atoms in the alloy require higher energy to move and to crystallize, and thus increases the thermal stability of amorphous alloys. On the other hand, the negative heat of mixing between Y and Al is as large as −38 kJ/mol [23], although the bonding forces between Y and the constituent elements Ti and Zr are weak, which can be expected to effectively slow down the Al diffusion and nucleation of FCC Al particles, and to enhance the thermal stability.

By integrating the exothermal peaks in the inset of Fig. 3, the crystallized volume fraction (x) as a function of temperature (T) can be obtained, as shown in Fig. 4. The slope of the x–T curves is corresponding to the crystallization rate under a constant heating rate. For the present samples, all the x–T curves at the different heating rates show a typical "S" shape, which indicated that the crystallization rate was relatively slow at both the beginning and the final, while it became large when the crystallization fraction was between 20% and 80%. This is because the atoms of the amorphous alloy became more and more active as the temperature increased, leading to some clusters formed by the atoms having high appetencies. At the early stage of crystallization, the nucleation rate was low because of relatively low diffusion speed. When the temperature reached at a certain value, the activation energy became large enough to induce reaction to occur among the elements. Hence the crystalline nuclei formed and the crystallization process was accelerated. Subsequently, the process gradually slowed down due to decreased nucleation sites. The similar evolution has been observed in the preliminary investigations on the amorphous materials during the non-isothermal crystallization processes [19,24]. It can also be found that the x–T curves shift to right along the temperature axis with the increase of heating rate, which is a typical behavior of the thermally

Table 1
Characteristic temperatures and kinetic parameters for the $Al_{76}Ni_8Ti_8Zr_4Y_4$ glassy powder determined by non-isothermal analysis.

	β (K/min)			
	15	20	30	40
T_g (K)	706	726	736	750
T_x^{onset} (K)	792	796	802	808
T_x^{peak} (K)	806	811	817	824
ΔT_x (K)	86	70	66	58

Table 2
Atomic mixing enthalpies (kJ/mol) and radii mismatch (%) for Al, Ni, Ti, Zr, and Y binary systems.

	E_{ak} (kJ/mol)	E_{ao} (kJ/mol)	K_0 (min^{-1})
T_g (K)	89	96	1.1×10^6
T_x^{onset} (K)	316	312	5.5×10^{20}
T_x^{peak} (K)	293	291	8.2×10^{18}

driven processes. Meanwhile, the inoculation time of crystallization increased with increasing heating rates, which implies that the resistance for nucleation of the crystallization event with higher heating rate is larger than that with the lower heating rate.

The activation energy is usually defined as an energy barrier against crystallization reaction. The apparent activation energy, E_a, for the observed crystallization temperatures can be determined by the Kissinger's or Ozawa's equation in the following form [25,26]:

$$\ln\left(T^2/\beta\right) = E_a/RT + \ln(E_a/k_0R) \text{ or} \tag{1}$$

$$\ln\beta = -1.0516E_a/RT + C_1 \tag{2}$$

where β is the heating rate, R is the gas constant, T is the peak temperature, C_1 is a constant, and K_0 is the frequency factor in Arrhenius equation, which is the probability that an atom having energy E_a will participate in a crystallization reaction.

Therefore, by substituting T_x^{onset} and T_x^{peak} for T in Eqs. (1) and (2), the activation energy for crystallization can be determined from the slope of a plot of $\ln(T^2/\beta)$ or $\ln(\beta)$ against $1/T$. The curves are shown in Fig. 5. As shown in Fig. 5, Kissinger's and Ozawa's curves are approximately straight lines, suggesting that only one reaction mechanism is operative in this range of heating rates. The values of frequency factor (K_0) and apparent activation energies calculated by the Kissinger (E_{ak}) and Ozawa (E_{ao}) equations are listed in Table 3. Obviously, the two equations yield almost the same apparent energy, confirming the reliability of the data. The estimated activation energy from the onset crystallization temperature is about 316 kJ/mol calculated by Kissinger's analysis. It is higher than those observed in Al–TM–TM (TM: transition metals) amorphous alloys investigated by other researchers [27–29]. Higher crystallization activation energies generally favor thermal stability. The very large apparent activation energy for crystallization indicates that atomic diffusion in Al–Ni-Ti–Zr–Y system is very difficult, therefore, the addition of Y improves the ability to resist crystallization of the present alloy.

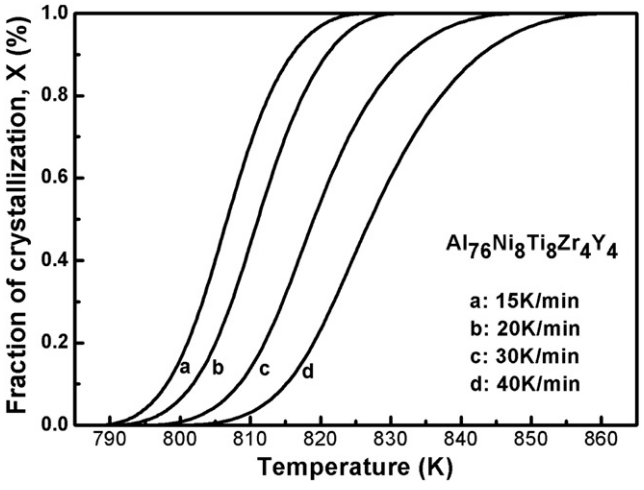

Fig. 4. Crystallization volume fraction as a function of annealing temperature.

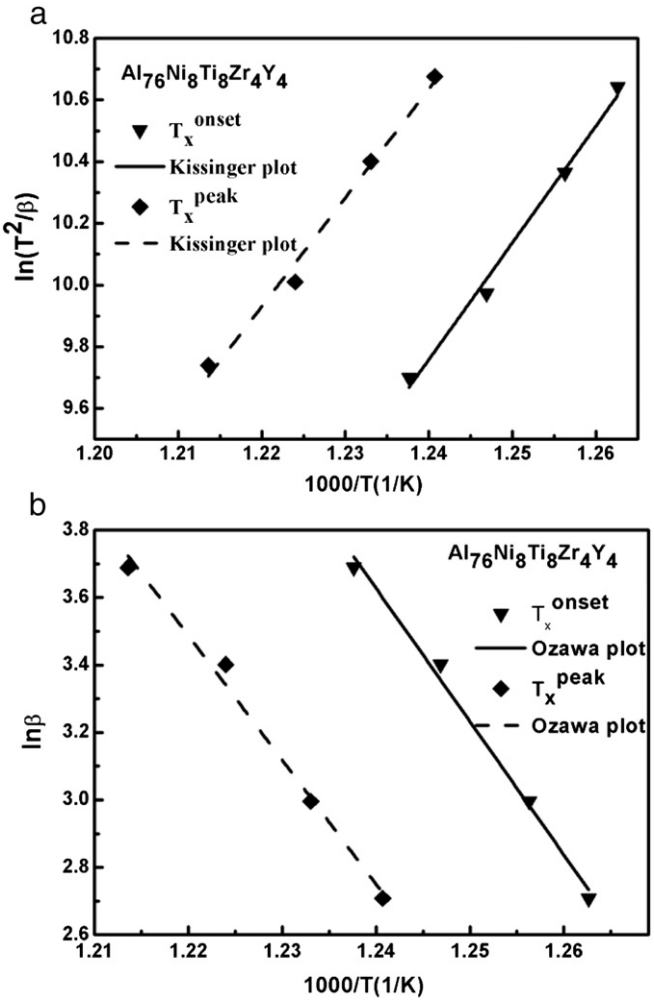

Fig. 5. (a) Kissinger plots and (b) Ozawa plots of the $Al_{76}Ni_8Ti_8Zr_4Y_4$ glassy power milled for 120 h.

The local activation energy means the activation energy at a stage when the crystallized volume fraction is x, which reflects the changes of nucleation and growth during the crystallization process. It can be determined by Flynn–Wall–Ozawa (*FWO*) relation [30], i.e.

$$\ln \beta = -1.0516 E_a(x)/RT(x) + C_2 \tag{3}$$

where $E_a(x)$ is the local activation energy when the crystallization fraction is x, C_2 is a constant, and $T(x)$ is the temperature corresponding to x. The $E_a(x)$ values for different crystallization fractions can be calculated from the slope of $\ln\beta$ vs. $1/T$ plot. The dashed line is a fitted curve with the $E_a(x)$ data points. As shown in Fig. 6, the local activation energy tends to decrease monotonically with increasing the crystallization volume fraction. It indicates that the process of crystallization is more easily as the temperature or crystallization fraction increases and the average value (261 kJ/mol) is less than that evaluated from the

Table 3
The frequency factor (K_0) and the apparent activation energies calculated by the Kissinger (E_{ak}) and Ozawa (E_{ao}) equations.

	Al	Ni	Ti	Zr	Y
Al	–	12.6%	2.1%	10.1%	19.7%
Ni	−22 kJ/mol	–	14.0%	21.4%	29.8%
Ti	−30 kJ/mol	−35 kJ/mol	–	8.8%	18.50%
Zr	−44 kJ/mol	−49 kJ/mol	0 kJ/mol	–	10.7%
Y	−38 kJ/mol	−31 kJ/mol	15 kJ/mol	9 kJ/mol	–

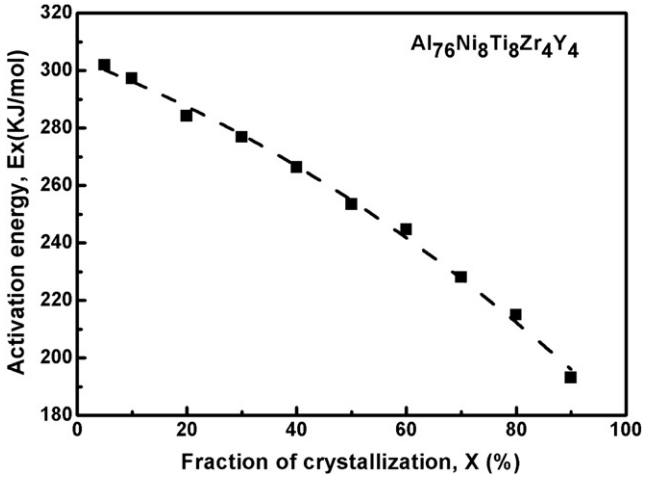

Fig. 6. Variation of the local activation energy with the crystallization volume fraction derived from the FWO equation.

Kissinger's and Ozawa equations. The difference may be due to the exothermic reaction during the process of crystallization.

The apparent activation energy E_a is in fact composed of two parts: nucleation and growth with respect to the activation energy, E_n and E_g, respectively [31]. The early stage of crystallization is expected to be dominated by the nucleation process for a crystalline phase, and the final stage of the crystallization depends on the growth process. According to the intercept of the vertical ordinate, the activation energy for nucleation can be obtained $E_n = E_x(0) = 304$ kJ/mol. Likewise, the activation energy for growth can be get $E_g = E_x(100\%) = 179$ kJ/mol, which is a little higher than the activation energy of self-diffusion of Al atoms in both a crystalline and amorphous matrix of about 140 kJ/mol. This possibly implies that the crystal growth of FCC Al phase was governed by Al atom diffusion in the Al-based matrix.

As is known, the Avrami exponent n gives detailed information on the nucleation and growth mechanism of new crystalline grains during the phase transition, which can be obtained by the extensively used Johnson–Mehl–Avrami (*JMA*) equation [32]:

$$x = 1 - \exp\left[-(kt)^n\right] \tag{4}$$

where x is the crystallization volume fraction at time t, n is the Avrami exponent related to the nucleation and growth and k is the reaction rate constant related to absolute temperature described by Arrhenius equation:

$$k = k_0 \exp(-E_a/RT) \tag{5}$$

where k_0 is a constant, E_a is the activation energy, R is the gas constant and T is the absolute temperature. However, the *JMA* equation is only suitable for isothermal crystallization process, the Avrami exponent of the non-isothermal process can be obtained as follows [33]:

$$n(x) = \frac{-R\partial \ln[-\ln(1-x)]}{E_a(x)\partial \ln(1/T)} \tag{6}$$

by which the local Avrami exponent $n(x)$ can be obtained according to the local activation energy $E_a(x)$. Fig. 7 shows the local Avrami exponent as a function of crystallization volume fraction at the heating rate of 30 K/min. It can be seen that the Avrami exponent decreased as temperature increased.

According to the diffusion-controlled growth behavior as discussed in Refs. [34,35], $n > 2.5$ means the growth of small particles with an increasing nucleation rate; $n = 2.5$ pertains to the growth of small particles with a constant nucleation rate; $1.5 < n < 2.5$ reflects the growth of

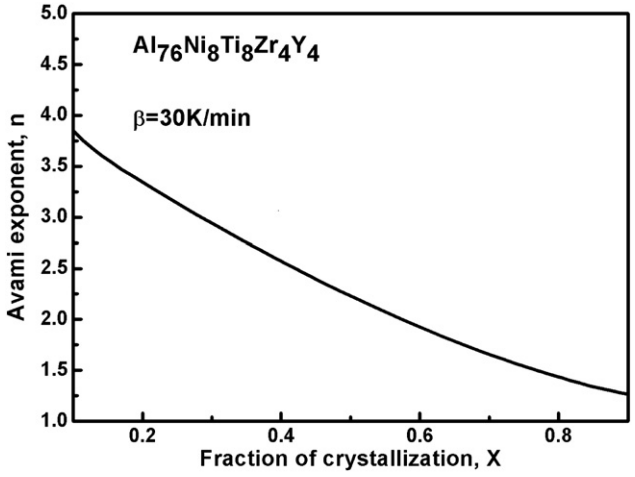

Fig. 7. The Avrami exponent as a function of crystallized volume fraction at a heating rate of 30 K/min.

small particles with a decreasing nucleation rate; n = 1.5 stands for the growth of small particles with a nucleation rate close zero; $1 < n < 1.5$ indicates different kinds of growth of pre-existing nuclei. The values of n of the present $Al_{76}Ni_8Ti_8Zr_4Y_4$ glassy powder decreased from 3.85 to about 1.25, and then the crystallization process can be divided into two stages, at the beginning of the primary crystallization ($0.1 < x < 0.75$), the $n(x)$ is in the range of 1.5–3.85, which means the two- and three-dimensional nucleation and grain growth controlled by diffusion with a decreasing nucleation rate. In the second stage ($0.75 < x < 0.9$), the $n(x)$ decreases to be around 1.25 with the increasing crystallized fraction, which indicates that there are a large number of the crystal nuclei growing up directly. From the variation of the Avrami exponent, the growth kinetics of nanocrystals during crystallization is strongly affected by unequal component diffusivities.

Thermal stability of the metallic glasses is one of the most important properties influencing their application. Due to the two parameters T_x^{onset} and ΔT_x that vary with heating rate, thus using them to evaluate the thermal stability of an amorphous alloy is not enough. Recently, some researchers conducted studies to evaluate the long-term thermal stability through an extension of the Kissinger analysis [36]. Fig. 8 (solid line) shows the CHT of the present $Al_{76}Ni_8Ti_8Zr_4Y_4$ glassy powder with the time axis in decimal logarithmic coordinates. The dashed line in Fig. 8 indicates a situation at the heating rate of 30 K/min. It is found that the lower the service temperature the longer period needed for the devitrification process, given that the service temperature is 700 K, the endurance time is longer than 10^3 ks. While the service temperature decreases to 500 K, the time to resist the devitrification is longer than $8.26 * 10^{11}$ ks. Thus, the glassy powder will devitrify even at room temperature at sufficiently large time scale, indicating the present $Al_{76}Ni_8Ti_8Zr_4Y_4$ alloy is thermally stable indeed at room temperature.

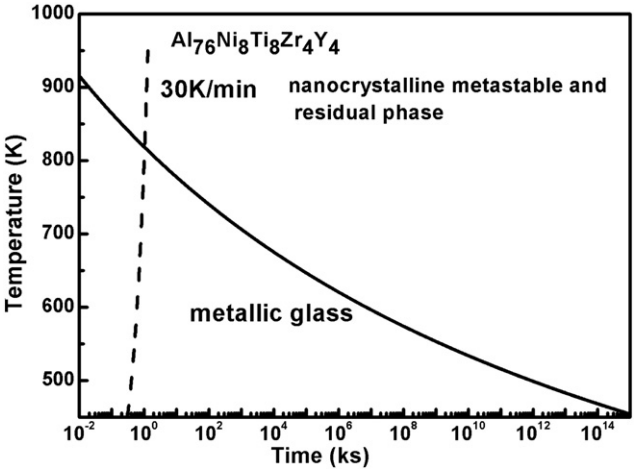

Fig. 8. Continuous heating transformation diagram of the $Al_{76}Ni_8Ti_8Zr_4Y_4$ glassy powder, where the dashed vertical line represents a heating rate of 30 K/min.

Although long-term thermal stabilities of different metallic glasses have been done using CHT diagrams, so far very little work to verify the results, especially long time annealing than 10 ks. To convince the thermal stability for a very long period of time, a quick annealing of the glassy powder at 700 K for 24 h (~10^2 ks) was conducted. The XRD pattern was also shown in Fig. 2. It can be seen that the glass powder retains halo diffraction peaks corresponding to the amorphous structure, superimposed by the Bragg diffraction peaks with very weak intensity, indicating that the percentage of crystalline phase is low. However, the annealing time is much less than ~$10^{\wedge 3}$ ks according to Fig. 8. Therefore the corollary of Kissinger analysis seems to be not valid for the estimation of long-term stability of the present alloy and our further investigations are underway.

4. Conclusions

Amorphous $Al_{76}Ni_8Ti_8Zr_4Y_4$ powder was obtained by mechanical alloying. The thermal stability and the thermal parameters are enhanced greatly by Y addition, because of the appropriate atomic-size mismatch and the negative heat of mixing between Y and Al. The present glassy power devitrified by a single stage crystallization mode, the crystallized products are FCC Al, AlTi, $AlTi_3$ Al_2Y and Al_3Zr. The dominating crystallization mechanism of the present alloy is two- and three-dimensional nucleation and growth controlled by diffusion with a decreasing nucleation rate. The apparent activation energy for the crystallization determined by both the Kissinger and Ozawa equations, revealed a similar value in the range of 290 and 316 kJ/mol. Though the long-term thermal stabilities of the present alloy does not accord with the CHT diagrams, the present glass powder has a large SLR ΔT_x values and good long-term thermal stability, which is beneficial for the consolidation of mechanically alloyed powders by powder metallurgy processing.

Acknowledgments

This work is jointly supported by the knowledge innovation project of Hefei Institutes of Physical Science, Chinese Academy of Sciences in the No. Y04N531124, the National Basic Research Program of China in the No. 2011CB610300, the National Natural Science Foundation of China in the No. 51371167, and the Foundation of President of Hefei Institutes of Physical Science, Chinese Academy of Sciences in the No. Y14N54B21.

References

[1] A. Inoue, Prog. Mater. Sci. 43 (1998) 365–520.
[2] Y.F. Ouyang, L.Y. Wang, H.M. Chen, X.Y. Cheng, X.P. Zhong, Y.P. Feng, J. Non-Cryst. Solids 354 (2008) 5555–5558.
[3] H. Yang, K.Y. Lim, Y. Li, J. Alloy. Compd. 489 (2010) 183–187.
[4] L. Wang, L. Ma, H. Kimura, A. Inoue, Mater. Lett. 52 (2002) 47–52.
[5] Y. Wang, X.X. Chen, H.R. Geng, Z.X. Yang, J. Alloy. Compd. 474 (2009) 152–157.
[6] H.W. Yang, M.J. Tan, R.V. Ramanujan, Scr. Mater. 66 (2012) 382–385.
[7] B.J. Yang, J.H. Yao, J. Zhang, H.W. Yang, J.Q. Wang, E. Ma, Scr. Mater. 61 (2009) 423–426.
[8] Y.D. Dong, W.H. Wang, K.Q. Xiao, L. Liu, S.H. Tong, Y.Z. He, Structural investigation of mechanically alloyed Al–Fe system, Mater. Sci. Eng. A 134 (1991) 867–871.
[9] W.H. Wang, K.Q. Xiao, Y.D. Dong, Y.Z. He, A study on mechanically alloyed amorphous $Al_{20}Fe_{80}$ powder by X-ray diffraction and Mössbauer spectroscope, J. Non-Cryst. Solids 124 (1990) 82–85.
[10] G.Q. Xie, D.V. Louzguine-Luzgin, H. Kimura, A. Inoue, Appl. Phys. Lett. 90 (2007) 241902-1–241902-3.
[11] K.B. Surreddi, S. Scudino, M. Sakaliyska, K.G. Prashanth, D.J. Sordelet, J. Eckert, J. Alloy. Compd. 491 (2010) 137–142.
[12] X.P. Li, M. Yan, H. Imai, K. Kondoh, J.Q. Wang, G.B. Schaffer, M. Qian, Mater. Sci. Eng. A 568 (2013) 155–159.

[13] G.Q. Xie, D.V. Louzguine-Luzgin, A. Inoue, J. Alloy. Compd. 509S (2011) S214–S218.
[14] D.H. Bae, M.H. Lee, D.H. Kim, D.J. Sordelet, Appl. Phys. Lett. 83 (2003) 2312–2314.
[15] M.H. Lee, D.H. Bae, D.H. Kim, D.J. Sordelet, J. Mater. Res. 18 (2003) 2101–2108.
[16] J.Q. Wang, Y.H. Liu, S. Imhoff, N. Chen, D.V. Louzguine-Luzgin, A. Takeuchi, M.W. Chen, H. Kato, J.H. Perepezko, A. Inoue, Intermetallics 29 (2012) 35–40.
[17] X. Wei, X.F. Wang, F.S. Han, H.W. Xie, C.E. Wen, J. Alloy. Compd. 496 (2010) 313–316.
[18] J.M. Park, J.S. Park, J.H. Na, D.H. Kim, D.H. Kim, Mater. Sci. Eng. A 435–436 (2006) 425–428.
[19] X. Wei, X.F. Wang, X.F. Wang, F.H. Han, J. Mater. Sci. 45 (2010) 6593–6598.
[20] M. Salehi, S.G. Shabestari, S.M.A. Boutorabi, J. Non-Cryst. Solids 375 (2013) 7–12.
[21] X.P. Li, M. Yan, J.Q. Wang, H. Huang, C. Kong, G.B. Schaffer, M. Qian, J. Alloy. Compd. 530 (2012) 127–131.
[22] L. Stojanova, K. Russew, E. Fazakas, L.K. Varga, J. Alloy. Compd. 540 (2012) 192–197.
[23] A. Takeuchi, A. Inoue, Mater. Trans. 46 (2005) 2817–2829.
[24] Y. Wang, K. Xu, Q. Li, J. Alloy. Compd. 540 (2012) 6–15.
[25] H.E. Kissinger, Anal. Chem. 29 (1957) 1702–1706.
[26] T. Ozawa, J. Therm. Anal. 2 (1970) 301–310.
[27] D.H. Kim, W.T. Kim, D.H. Kim, Mater. Sci. Eng. A 385 (2004) 44–53.
[28] K.L. Sahoo, M. Wollgarten, J. Haug, J. Banhart, Acta Mater. 53 (2005) 3861–3870.
[29] M. Gogebakan, P.J. Warren, B. Cantor, Mater. Sci. Eng. A 226–228 (1997) 168–172.
[30] J.H. Flynn, J. Therm. Anal. 27 (1983) 95–103.
[31] K. Lu, J.T. Wang, Mater. Sci. Eng. A 133 (1991) 500–503.
[32] J.M. Barandiarán, I. Tellería, J.S. Garitaonandía, H.A. Davies, J. Non-cryst. Solids 329 (2003) 57–62.
[33] W. Lu, B. Yan, W.H. Huang, J. Non-Cryst. Solids 351 (2005) 3320–3324.
[34] N.X. Sun, X.D. Liu, K. Lu, Scr. Mater. 34 (1996) 1201–1207.
[35] S. Scudino, S. Venkatarama, J. Eckert, J. Alloy. Compd. 460 (2008) 263–267.
[36] D.V. Louzguine, A. Inoue, Scr. Mater. 47 (2002) 887–891.